

# Evaluation of Hepatocellular Carcinoma With Dynamic $^{11}\text{C}$ -Acetate PET: A Dual-Modeling Method

Sirong Chen and Dagan Feng, *Fellow, IEEE*

**Abstract**—Quantification of the  $^{11}\text{C}$ -acetate liver studies with dynamic positron emission tomography (PET) could significantly improve the evaluation of hepatocellular carcinoma (HCC), where both time-activity curves (TACs) of the hepatic artery (HA) and portal vein (PV) (the dual hepatic blood supply) are required. However, directly measuring them by the blood sampling or cannulation procedure is very invasive. In addition, it is very hard to differentiate the PV from the surrounding liver tissue on PET images by the currently developed indirect methods. To noninvasively and efficiently access the TAC of PV, we investigated the possibility of modeling the dual hepatic blood supply and presented two hepatic dual-input (DI) models. Combining the established  $^{11}\text{C}$ -acetate liver model with two different DI models, we obtained two dual-models with six/seven parameters to fit the dynamic PET measurements. The fitting results were compared with those of the  $^{11}\text{C}$ -acetate liver model using image-derived dual hepatic inputs (the “Golden standard”) by statistical study. The adequacy of the two dual-models was estimated by Akaike Information Criteria (AIC) and Schwarz Criteria (SC). It was revealed that the proposed modeling technique could successfully account for the hepatic dual blood supply and the six-parameter (6-P) dual-model is more suitable for quantification of  $^{11}\text{C}$ -acetate liver studies.

**Index Terms**—Dual-model, hepatic dual-input (DI) model, hepatocellular carcinoma (HCC), parameter estimation, positron emission tomography (PET).

## I. INTRODUCTION

THE use of positron emission tomography (PET) for the study of liver disease has been mainly in the detection of liver tumors [1]–[5]. However, the investigation of the well-established  $^{18}\text{F}$ -fluorodeoxyglucose (FDG) PET imaging suggested that the detection of liver tumors, especially hepatocellular carcinoma (HCC), is hampered due to the abundance of the

Manuscript received February 11, 2007; revised May 21, 2008. This work was supported in part by the studentship of the Hong Kong Polytechnic University and in part by the UGC and ARC grants.

S. Chen is with the Center for Multimedia Signal Processing, Department of Electronic and Information Engineering, The Hong Kong Polytechnic University, Hong Kong, and also with the Department of Nuclear Medicine and PET, Hong Kong Sanatorium and Hospital, Hong Kong (e-mail: sirongchen@hksh.com).

D. Feng is with the Center for Multimedia Signal Processing, Department of Electronic and Information Engineering, The Hong Kong Polytechnic University, Hong Kong, and also with the Biomedical and Multimedia Information Technology Group, School of Information Technologies, The University of Sydney, Australia (e-mail: enfeng@iee.polyu.edu.hk).

Color versions of one or more of the figures in this paper are available online at <http://ieeexplore.ieee.org>.

Digital Object Identifier 10.1109/TNS.2008.924075

enzyme glucose-6-phosphatase in HCC leading to leakage of FDG metabolites back to the circulation [1], [6]. This Achilles’ heel of PET in evaluating HCC has not been resolved until Ho *et al.* [4], [5] introduced  $^{11}\text{C}$ -acetate tracer in imaging HCC. The quantitative modeling studies of the dynamic  $^{11}\text{C}$ -acetate PET were thereafter conducted and the results conclusively shown that the measurement of the *local hepatic metabolic rate-constant of acetate (LHMRAc)* and the *relative portal venous contribution to the hepatic blood flow ( $a_v$ )* can provide important diagnostic information for detecting HCC [7], [8].

For the quantification of the dynamic  $^{11}\text{C}$ -acetate PET in liver, the tracer concentration of both hepatic artery (HA) and portal vein (PV) (the dual hepatic blood supply) should be considered as the model input [6]–[9]. Directly measuring them by the widely adopted catheterization and sampling procedure is invasive to the subject and exposes personnel to the risks associated with the handling of patient blood [10]. In addition, gaining access to the PV is impractical in clinical settings.

To eliminate the invasive blood sampling procedure, many indirect measurement methods have been developed. PET-acquired input function has been validated for various quantitative studies [11]–[16], where manual placement of the location of blood vessels is always required. Besides, some automatic procedures based on factor analysis, principal component analysis, independent component analysis, etc. [17], [18], were found efficient to extract the HA blood factor from the dynamic PET images. However, the tracer arriving at the PV is delayed and dispersed, and furthermore, the radioactivity spillover from the surrounding liver tissue to the PV is significant, making PV region indistinguishable from the surrounding liver tissue. Another type of solution to acquire the input function noninvasively is a modeling approach [19], [20]. Nevertheless, little attention has been paid to model the tracer kinetics in PV. The PV input function is generally predicted by convolution of the arterial input with a notional system function with five parameters [20]. However, estimating ten parameters simultaneously (including the five parameters of the  $^{11}\text{C}$ -acetate liver model [8]) would make the convergence very difficult.

In this work, our objective is to model the dual hepatic blood supply to eliminate the measurement of PV input function for quantitative liver studies with dynamic  $^{11}\text{C}$ -acetate PET (quantification of the two HCC indicators:  $a_v$  and *LHMRAc*). Two dual-models with six and seven parameters (6-P and 7-P) were proposed, whose input function was modeled to account for the dual hepatic blood supply. The performance of the two dual-models was evaluated by comparison with the  $^{11}\text{C}$ -acetate liver

model using image-derived TACs of HA and PV [8], which is the “best currently available” method in terms of accuracy and set as the “Golden standard” in this study.

## II. MATERIALS AND METHODS

### A. PET Examination

Dynamic  $^{11}\text{C}$ -acetate PET studies were performed on five human subjects including two with HCC, lying in the position that allows image acquisition of the liver dome and apical half of the left ventricle to the inferior part of liver. Immediately after the bolus intravenous injection of  $^{11}\text{C}$ -acetate, dynamic PET images were recorded by an ECAT EXACT 47 PET scanner (model 921; CTI/Siemens, Inc., Knoxville, TN), which simultaneously acquired 47 contiguous transverse slices (septa extended) over a period of 10 min by measuring ten 4 sec frames, eight 10 sec frames, two 30 sec frames, followed by three 60 sec frames and two 120 sec frames, a total of 25 frames. Reconstruction and attenuation correction were performed with the standardized ordered-subsets expectation maximization technique.

### B. Analysis of the $^{11}\text{C}$ -Acetate PET Images

For quantitative analysis, regions of interest (ROIs) were defined on a single transverse slice on a frame-by-frame basis. The TAC of each ROI was created by averaging the activity in each region. For each patient, two ROIs were defined, and thus, a total of eight nontumor liver tissue ROIs and two HCC ROIs (from the two HCC patients) were extracted from the images of the five patients. To be relatively free of the radioactivity spillover from the liver tissue, the TAC of HA was approximated by defining ROI over the abdominal aorta (relatively far from the liver), which is within the region of little  $^{11}\text{C}$ -acetate activity. The TAC of PV was obtained by direct PET measurements with the help of experienced clinicians or the CT reference [7]. Partial volume effect correction is not considered necessary since the diameters of normal aorta and PV (in the order of 2–3 cm and 1–2 cm, respectively), and the selected tumor sizes (2–3 cm) are safely above the smallest resolution capacity of the PET scanner ( $\sim 0.5$  cm).

### C. Modeling the Dual Hepatic Blood Supply

As aforementioned, in contrast to other organs or tissues, which are supplied only by arterial blood, the liver has a dual source of blood supply: receiving oxygenated blood from the common left and right HAs and nutrient-rich blood from the gastrointestinal (GI) tract via the PV [7]. In this study, we presented a one-compartment model (upper left of Fig. 1) with the blood TACs in aorta and PV ( $c_v(t)$  (Bq/ml)) as the model input and output, respectively. When the tracer concentration of the arterial blood entering the GI tract was approximated to that of HA ( $c_a(t)$  (Bq/ml)), according to Fick principle, we obtain

$$\frac{dQ_g(t)}{dt} = F(c_a(t) - c_v(t)) - EQ_g(t) \quad (1)$$

where  $Q_g(t)$  (Bq) is the quantity of  $^{11}\text{C}$ -acetate in the GI tract,  $F$  is the net extraction rate constant of tracer down the GI tract, and it was assumed that the arterial flow was equal to the venous flow, denoted by  $F$  (ml/min). An assumption was also made that the blood in the GI tissue forms only a small percentage of the total tissue volume. If  $V$  (ml) denotes the volume of the GI tissue, then the differentiation of the  $^{11}\text{C}$ -acetate concentration in the GI tissue ( $c_g(t)$ ) could be given by

$$\frac{dc_g(t)}{dt} = \frac{1}{V} \frac{dQ_g(t)}{dt} = \frac{F}{V} (c_a(t) - c_v(t)) - \frac{E}{V} Q_g(t) \quad (2)$$

and we also assume that  $^{11}\text{C}$ -acetate is a freely diffusible tracer in the circulation, which diffuses rapidly between blood and tissue. Therefore,  $c_g(t)$  could be approximated by

$$c_g(t) = \lambda c_v(t) \quad (3)$$

where  $\lambda$  is the partition coefficient describing ratio of the solubility of  $^{11}\text{C}$ -acetate in the GI tissue and blood [21]. Substituting  $c_g(t)$  in (2) with (3), we have

$$\frac{\lambda dc_v(t)}{dt} = \frac{F}{V} (c_a(t) - c_v(t)) - \lambda E c_v(t). \quad (4)$$

Then, the differentiation of  $c_v(t)$  could be expressed as

$$\frac{dc_v(t)}{dt} = \frac{F}{\lambda V} (c_a(t) - c_v(t)) - E c_v(t). \quad (5)$$

Take the Laplace transform of (5), and then take the inverse Laplace transform,  $c_v(t)$  could be predicted by

$$c_v(t) = p e^{-(p+E)t} \otimes c_a(t), \quad p = \frac{F}{\lambda V} \quad (6)$$

where  $\otimes$  denotes the operation of temporal convolution.

In the previous quantitative PET studies in liver [8], the dual-input function  $c_b(t)$  of the  $^{11}\text{C}$ -acetate liver model was calculated by

$$c_b(t) = (1 - a_v) \times c_a(t) + a_v \times c_v(t) \quad (7)$$

where  $a_v$  is the “relative portal venous contribution to the hepatic blood flow”, one of the HCC indicators [8]. Substitute  $c_v(t)$  in (7) with (6), we have

$$c_b(t) = (1 - a_v) \times c_a(t) + a_v \times (p e^{-(p+E)t} \otimes c_a(t)) \quad (8)$$

where  $a_v$ ,  $p$  (/min) and  $E$  are the parameters of the hepatic DI model. In this study, we also investigated the possibility of simplifying  $E$  to be zero since there is little  $^{11}\text{C}$ -acetate activity in GI tract on PET images by visual judgment.

### D. Parameter Estimation for the $^{11}\text{C}$ -Acetate Dual-Model

The hepatic dual-input function (8) would serve as the input of the established  $^{11}\text{C}$ -acetate liver model (Please refer to Appendix A), and these two models together would be named as “ $^{11}\text{C}$ -acetate dual-model” (Fig. 1). Combining the above-stated (8) and (4) in Appendix A, all the dual-model parameters ( $a_v$ ,  $p$ ,  $E$ ,  $K_1$ ,  $k_2$ ,  $k_3$  and  $HBV$ ) (named 7-P dual-model) could be estimated theoretically using image-derived  $c_a(t)$  and  $c_T(t)$  as

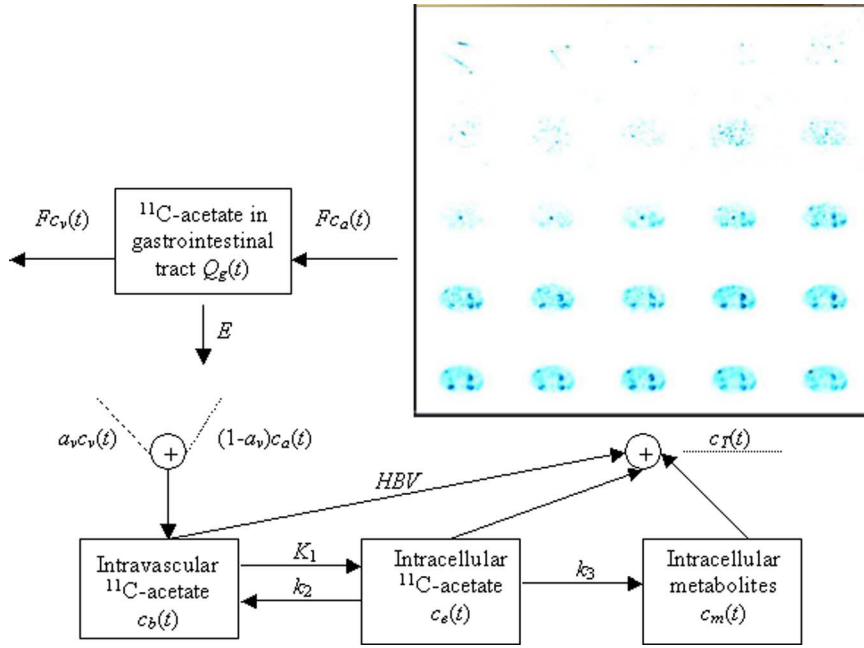


Fig. 1. Skeleton of the presented dual-model of  $^{11}\text{C}$ -acetate in liver. The serial images at the upper right are the typical dynamic  $^{11}\text{C}$ -acetate PET images in liver. The one-compartment model shown at the upper left represents the hepatic dual-input model (DI). The dual-input function obtained from this DI model serves as the input of the  $^{11}\text{C}$ -acetate liver model shown at the bottom.  $HBV$  is the “hepatic blood volume” term.  $K_1$  (ml/min/ml) represents the first order rate constant for the transport of  $^{11}\text{C}$ -acetate from blood to tissue,  $k_2$  (/min) for reverse transport of  $^{11}\text{C}$ -acetate from tissue to blood and  $k_3$  (/min) for conversion of  $^{11}\text{C}$ -acetate to its products/metabolites.

the model input and output. If Parameter  $E$  of the hepatic DI model could be neglected, the dual-model will have six parameters, and is thus named as 6-P dual-model.

Since a relatively large number of parameters need to be estimated, for more reliable parameter estimation, the graphed nonlinear least squares (GNLS) algorithm (Please refer to Appendix B) [22] rather than the conventional NLS approach was used. The flow chart of the estimation procedure by GNLS for the  $^{11}\text{C}$ -acetate dual-model was shown in Fig. 2.

The individual parameters of the established 5-P model with image-derived dual inputs were estimated by NLS method and Parameter  $LHMRAct$  (same form as the forward clearance  $K = K_1 k_3 / (k_2 + k_3)$ ) was estimated by Patlak method [23], which is the “best currently available” method.

#### E. Statistical Analysis

In this study, the performance of the  $^{11}\text{C}$ -acetate dual-model was tested by series of statistical analysis. To test the parameter identifiability, the covariance matrix ( $C$ ) was estimated based on sensitivity functions (partial derivatives of the measured states with respect to the estimated parameters). Under the assumption of uncorrelated measurement noise with Gaussian distribution with a mean of zero, the covariance matrix can also be approximated by the inverse of the Fisher information matrix (FIM) defined as [24], [25]

$$\text{FIM}(P) = \sum_{i=1}^N \left( \frac{\partial y_i}{\partial P}(P) \right)^T V^{-2} \left( \frac{\partial y_i}{\partial P}(P) \right) \quad i = 1, 2, \dots, 25 \quad (9)$$

where  $y_i$  is the fitted output,  $P$  is the parameters to be estimated and  $N$  is the number of data points. With the covariance matrix ( $C$ ), the correlation between the estimated parameters can be

obtained by the coefficient matrix ( $R$ ), whose elements are the approximate correlation coefficients ( $R_{ij}$ ) between the  $i$ -th and  $j$ -th parameters, defined by

$$R_{ij} = \frac{C_{ij}}{\sqrt{C_{ii}C_{jj}}}, \quad i \neq j \\ R_{ii} = 1, \quad i = j. \quad (10)$$

A singular FIM indicates the presence of unidentifiable parameters, and correlations between parameters that are greater than 0.99 may lead to singular FIM.

Coefficient of variation (CV), which is the computed measurements of the estimates’ variability, was used to statistically examine the estimation reliability. The CV was calculated by

$$\text{CV} = \frac{\text{SD}}{P} \times 100\% \quad (11)$$

where SD is the standard deviation of the estimated parameter. During the non-linear regression of the clinical datasets, SD was estimated as the square roots of the diagonal elements of the covariance matrix ( $C$ ).

The estimation accuracy of the two HCC indicators ( $LHMRAct$  and  $a_v$ ) of the dual-model was tested by bias

$$\text{Bias} = \left| \frac{P^D - P^S}{P^S} \right| \times 100\% \quad (12)$$

where  $P^D$  is the dual-model estimate and  $P^S$  is the estimate of the established 5-P  $^{11}\text{C}$ -acetate liver model with image-derived TACs of HA and PV, which is the “Golden standard” method. Correlation analysis was conducted among the estimation results of the three models in this study.

Akaike Information Criteria (AIC) [26] and Schwarz Criteria (SC) [27] were used to test the adequacy of the 6-P and 7-P

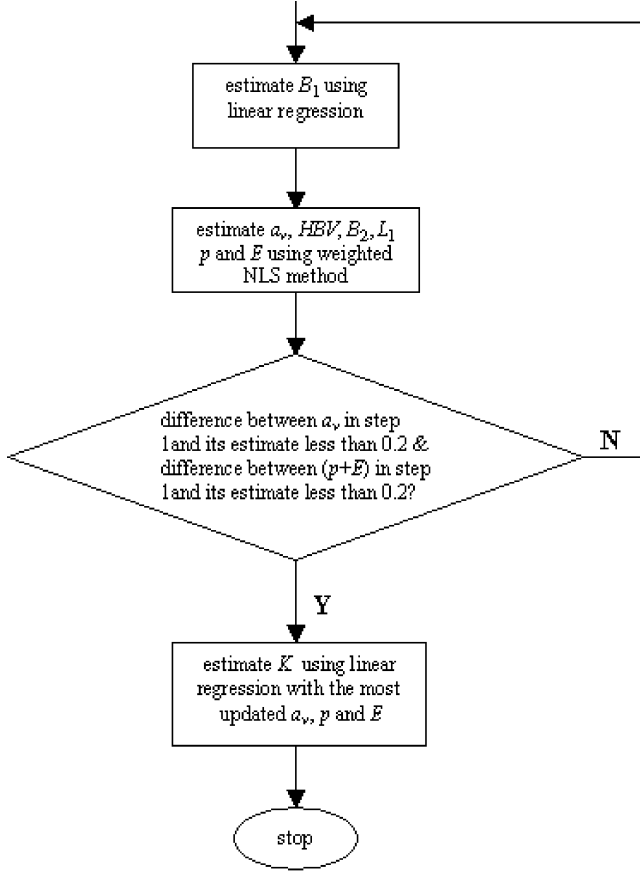


Fig. 2. Flow chart of the estimation procedure for the  $^{11}\text{C}$ -acetate dual-model using GNLS method.

dual-models. It was assumed that the data variances were known up to a proportionality constant, therefore the AIC and SC were given by

$$\text{AIC} = N \ln(WRSS) + 2N_P \quad (13)$$

$$\text{SC} = N \ln(WRSS) + N_P \ln N \quad (14)$$

where  $N_P$  is the number of parameters and  $WRSS$  is the weighted residual sum of squares between the fitted curves and PET measurements.

#### F. Simulation Study

To test the effectiveness of the proposed dual-model, computer simulation study was performed as well. One HCC and two normal liver tissue datasets were generated using three image-derived TACs of HA (decay corrected). A pseudo-random number generator was applied to generate the Gaussian noise which was added to the calculated TAC and the variance structure was described as

$$\sigma^2(t_i) = \frac{\alpha \times c_T(t_i)}{\Delta t_i} \quad i = 1, 2, \dots, 25 \quad (15)$$

where  $t_i$  is the sampling time of the clinical examination in this study,  $c_T(t_i)$  is the calculated PET measurement at  $t_i$ ,  $\sigma^2(t_i)$  is the variance of  $c_T(t_i)$ , and  $\alpha$  is the proportional constant representing the noise level, which was set to be 0.1, 0.5 and 1 in this simulation [19]. The estimation reliability was examined by CV

TABLE I  
RESULTS OF THE ESTIMATED  $a_v$  AND  $K$  OF THE 5-P  $^{11}\text{C}$ -ACETATE LIVER MODEL (WITH IMAGE-DERIVED TACs OF HA AND PV), AND THE 6-P, 7-P DUAL-MODELS (WITH IMAGE-DERIVED ARTERIAL TAC) FOR THE CLINICAL DATASETS

Datasets Number <sup>1</sup>	5-P model		6-P dual-model		7-P dual-model	
	$a_v$	$K$	$a_v$	$K$	$a_v$	$K$
1	0.9004	0.1642	0.9127	0.1651	0.8796	0.1764
2	0.9276	0.1763	0.9188	0.1771	0.9197	0.1895
3	0.8634	0.1587	0.8482	0.1496	0.8630	0.1576
4	0.7053	0.1773	0.7108	0.1713	0.7255	0.1903
5	0.6972	0.1483	0.7357	0.1402	0.7231	0.1422
6	0.7174	0.1552	0.7316	0.1506	0.7481	0.1549
7	0.8944	0.1739	0.8636	0.1829	0.8796	0.1975
8 <sup>2</sup>	0.3330	0.2728	0.3449	0.2962	0.3199	0.3005
9	0.8657	0.1898	0.9175	0.1742	0.9066	0.1756
10 <sup>2</sup>	0.5684	0.5066	0.5312	0.4666	0.5555	0.4633

Notes: 1. Two ROIs were extracted from each patient. The datasets were numbered like this: 1 and 2 from patient 1, 3 and 4 from patient 2 and so on. 2. Datasets 8 and 10 represent HCC.

and the estimation accuracy was evaluated by bias, which was calculated by

$$\text{Bias} = \left| \frac{P^{\text{true}} - \bar{P}}{P^{\text{true}}} \right| \times 100\% \quad (16)$$

where  $P^{\text{true}}$  is the true value of the parameter, and  $\bar{P}$  is the mean value of the estimated parameter. The global parameter identifiability was evaluated by (10).

### III. RESULTS AND DISCUSSION

Although image-derived method for the acquisition of hepatic dual-input is tedious and operator-dependent in routine clinical use, it is adopted as the “best currently available” method for dynamic  $^{11}\text{C}$ -acetate PET study in the liver in terms of accuracy [8]. Therefore, the 5-P model with image-derived dual-input was set as the “Golden standard” in this dual-modeling study. The estimation results of the two HCC indicators by the 6-P and 7-P dual-models and the “Golden standard” were summarized in Table I. The estimated  $a_v$  and  $K$  of both dual-models show significant difference between nontumor liver tissue and HCC ( $P \ll 0.05$ ). The estimation accuracy of  $a_v$  of the two dual-models in terms of bias is generally satisfactory (most bias values  $< 5\%$ ), especially for the 7-P dual-model, whose bias values are all less than 5%. The estimation accuracy of  $K$  of the 6-P dual-model is generally more satisfactory than that of the 7-P dual-model. The correlation coefficient of the estimated  $a_v$  between the 5-P and 6-P models is 0.9888; between the 5-P and 7-P models, it is 0.9930. For the estimation of  $K$ , the correlation coefficient of  $K$  is 0.9900 between the 5-P and 6-P models; for the 5-P and 7-P models, it is 0.9861. Therefore the parameter estimates of both dual-models correlate closely with those of the “Golden standard” respectively. The dual-models could account for the dual hepatic blood supply in terms of estimation accuracy.

Fig. 3 plots the calculated PV curves by the 6-P and 7-P dual-models versus the image-derived PV curve, indicating that

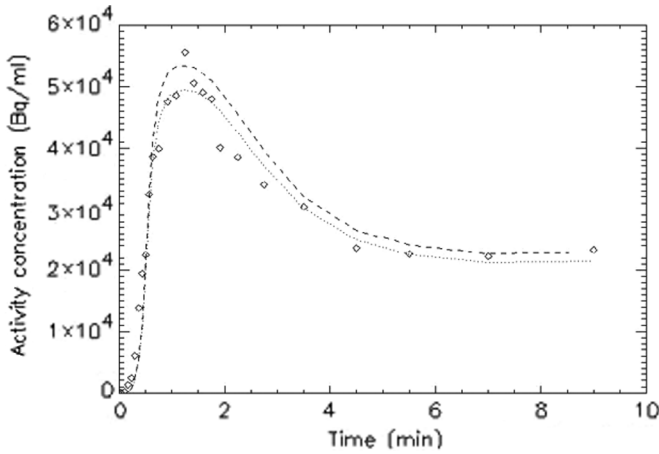


Fig. 3. Calculated PV curves by the 6-P (the dashed line) and 7-P (the dotted line) dual-models with estimated  $p$  and image-derived TAC of HA. The points denoted by symbol “diamond” are the image-derived PV measurements.

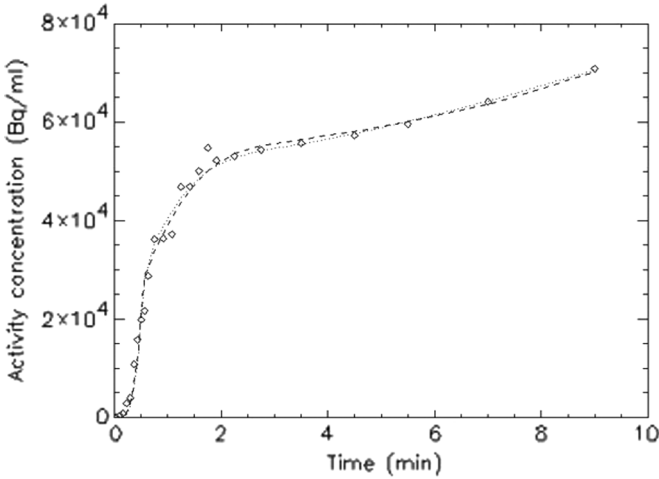
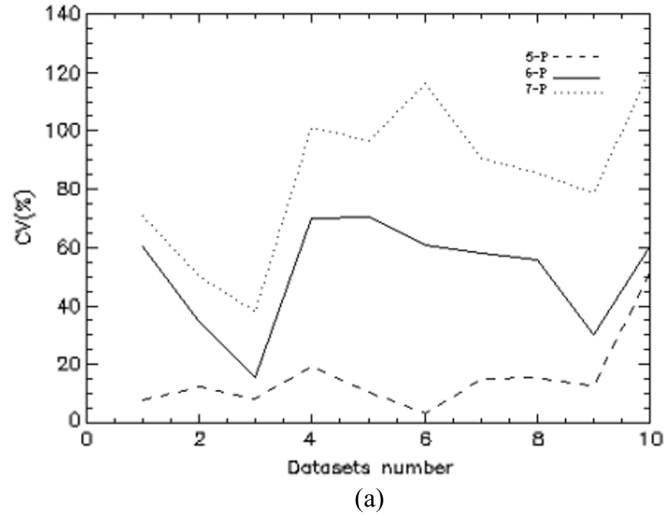


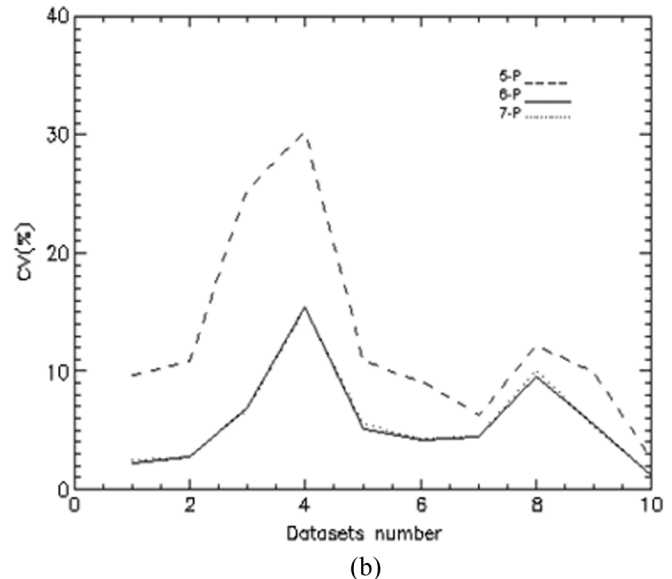
Fig. 4. Fitted TACs by the 6-P (dashed lines) and 7-P dual-models (dotted lines). The data denoted by symbol “diamond” represent the PET measurements (HCC case).

the 7-P dual-model could better match the PV measurements. However, the 6-P dual-model could provide better fitting accuracy at the later stage, which is very meaningful for the estimation of  $K$ . Fig. 4 shows an example of the fitted curves (HCC case) by the 6-P and 7-P dual-models, revealing that the 7-P dual-model could provide better fitting accuracy. Comparison of the estimation reliability in terms of CV of the three models was illustrated in Fig. 5. As shown in Fig. 5(a), the estimated  $a_v$  of both dual-models are less reliable than that of the 5-P model, which could be explained that more number of parameters to be estimated would reduce the estimation reliability. The reliability of the 6-P dual-model is acceptable since the average CV is less than 50%; whereas the reliability of the 7-P dual-model is far from satisfactory. Fig. 5(b) revealed that the estimated  $K$  of both dual-models is significantly more reliable than that of the “Golden standard” ( $P < 0.05$ ). Therefore, the 6-P dual-model could provide acceptable estimation reliability of  $a_v$  and more reliable estimation of  $K$  compared with the “Golden standard”.

Based on the results of identifiability analysis for clinical datasets, most estimates of  $a_v$  are identifiable from  $p$  of the 6-P



(a)



(b)

Fig. 5. Comparison of CV values of the estimated  $a_v$  (a) and  $K$  (b) of the 5-P model, 6-P and 7-P dual-models.

TABLE II  
ESTIMATION RESULTS OF  $p$  FOR THE 6-P DUAL-MODEL,  $p$  AND  
 $E$  FOR THE 7-P DUAL-MODEL BY GNLS METHOD

Datasets Number <sup>1</sup>	6-P dual-model		7-P dual-model			
	$p$	CV(%)	$p$	CV(%)	$E$	CV(%)
1	0.4743	51.65	0.4893	187.9	0.0369	121.9
2	0.4271	50.29	0.4024	218.1	0.0305	105.5
3	0.3292	23.91	0.3058	150.5	0.0200	201.5
4	0.3849	94.60	0.3502	164.9	0.0517	156.3
5	0.3671	42.34	0.3245	117.7	0.0341	191.5
6	0.4685	50.03	0.4786	163.1	0.0178	293.8
7	1.1816	92.74	1.1188	99.49	0.0770	119.1
8 <sup>2</sup>	1.1833	83.76	1.2143	161.9	0.1209	209.0
9	0.4750	33.31	0.4422	92.72	0.0205	234.4
10 <sup>2</sup>	0.5029	86.17	0.4695	207.0	0.0388	203.7

Notes: 1. Same as Table I.

2. Same as Table I.

dual-model; for the 7-P dual-model,  $a_v$  is generally identifiable from  $p$  and  $E$  respectively, and  $p$  is always identifiable from  $E$

TABLE III  
ESTIMATION RESULTS OF THE 6-P DUAL-MODEL USING GNLS METHOD FOR THREE SIMULATION STUDIES:  
(A) NORMAL LIVER TISSUE, (B) HCC, (C) NORMAL LIVER TISSUE. THE ESTIMATED PARAMETERS IN THIS TABLE REPRESENT  
THEIR *mean* VALUES. THE VALUES OF *mean*, bias, AND CV WERE CALCULATED FROM 100 SIMULATION RUNS

(a) true value:  $K_1 = 0.85, k_2 = 0.75, k_3 = 0.20, HBV = 0.30, a_v = 0.75, p = 1.00, K = 0.1789$

(b) true value:  $K_1 = 1.65$ ,  $k_2 = 0.70$ ,  $k_3 = 0.14$ ,  $HBV = 0.30$ ,  $a_v = 0.36$ ,  $p = 0.40$ ,  $K = 0.2750$

(c) true value:  $K_1 = 0.55, k_2 = 0.70, k_3 = 0.25, HBV = 0.22, a_v = 0.72, p = 1.00, K = 0.1447$

(all correlation coefficients  $<0.99$ ). The estimation results of  $p$  for the 6-P dual-model,  $p$  and  $E$  for the 7-P dual-model were listed in Table II. As shown in Table II, the two sets of estimated  $p$  are comparable to each other. For the 7-P dual-model, most estimated  $E$  values are less than 0.05 and most ratios of  $E$  to  $p$  are less than 10%. The 6-P dual-model could provide much more reliable estimation than the 7-P dual-model. The reliability of the estimated  $p$  for the 6-P dual-model is generally acceptable since most CVs are less than or around 50%. For the 7-P dual-model, both estimates of  $p$  and  $E$  are far from acceptable.

The correlation coefficients of the two sets of  $a_v$ ,  $K$  and  $p$  of the two dual-models are 0.9945, 0.9982 and 0.9961 respectively, indicating the parameter estimates of the two dual-models are linearly correlated. Therefore, inclusion (7-P) and exclusion of  $E$  (6-P) would have overall little impact on the estimation accuracy. In addition, 6-P dual-model could generally provide much more reliable estimation than 7-P dual-model. Therefore 6-P dual-model could be the more suitable transient system response in a 10-minute dynamic imaging.

To further evaluate the “goodness of fit” of the two dual-models, AIC and SC were utilized. It was shown that the 6-P dual-model has smaller AIC and SC values in all cases except the AIC value of region 8, suggesting that the 6-P dual-model is more suitable for quantification of the dynamic  $^{11}\text{C}$ -acetate liver studies.

Computer simulation was performed to test the effectiveness of the 6-P dual-model. Three simulation studies, including one HCC study, were conducted using three image-derived TACs of HA respectively. The GNLS estimation results of the *mean*, bias, and CV of the parameters  $K_1$ ,  $k_2$ ,  $k_3$ ,  $HBV$ ,  $a_v$ ,  $p$  and  $K$  (*LHMRAct*) of the 6-P dual-model calculated from 100 simulation runs were presented in Table III. As seen in Table III, all CVs are less than 20% for normal liver tissue cases and less than 36% for HCC case. All biases are less than or around 5%. Therefore, reliable and accurate parameter estimation could be provided by the 6-P dual-model with image-derived arterial input. Although the estimation of  $HBV$  and  $p$  is less reliable than that of the other parameters, the reliability is still acceptable. Con-

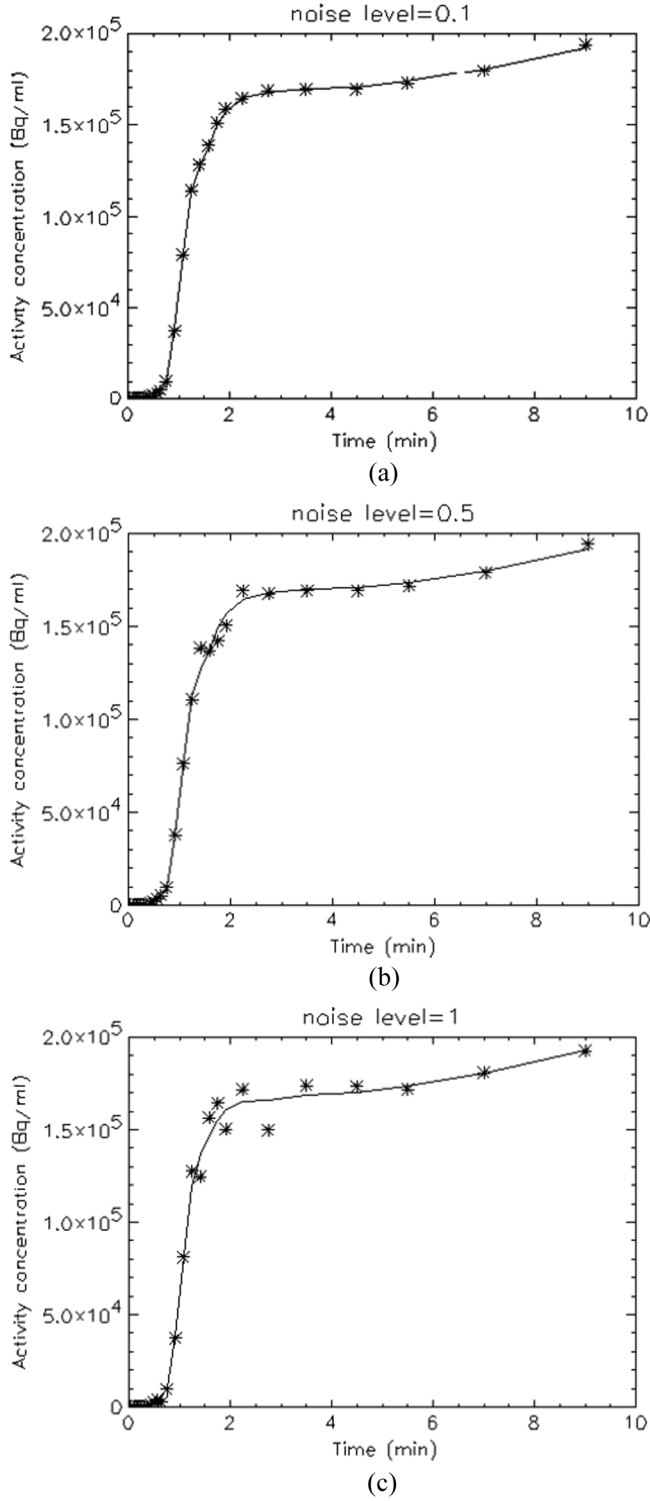


Fig. 6. Fitting results by the 6-P dual-model for the simulation data (HCC study) denoted by “asterisk” with noise levels 0.1 (a), 0.5 (b) and 1 (c).

cerning the two HCC indicators:  $LHMRAct$  (the forward clearance  $K$ ) and  $a_v$ , they could be accurately and reliably estimated, especially for Parameter  $K$ .

The fitting examples of the simulation study (HCC) of the 6-P dual-model with different noise levels: 0.1, 0.5, and 1 were drawn in Fig. 6. When comparing Fig. 4 with Fig. 6, it seems that the noise level of 1 is more similar with the noise level

TABLE IV  
CORRELATION COEFFICIENTS OF THE 6-P DUAL-MODEL PARAMETERS ON  
THE SIMULATED NORMAL (A) AND HCC (B) DATA (noise level = 1).  
THE CORRELATION COEFFICIENTS IN THIS TABLE REPRESENT  
THEIR MEAN VALUES FROM 100 SIMULATION RUNS

	$K_1$	$k_2$	$k_3$	$HBV$	$a_v$	$p$
$K_1$	-	0.46	0.48	0.21	0.21	0.45
$k_2$	-	-	0.51	0.75	0.75	0.97
$k_3$	-	-	-	0.70	0.72	0.98
$HBV$	-	-	-	-	0.99	0.77
$a_v$	-	-	-	-	-	0.77
$p$	-	-	-	-	-	-

(a)

	$K_1$	$k_2$	$k_3$	$HBV$	$a_v$	$p$
$K_1$	-	0.89	0.86	0.73	0.69	0.20
$k_2$	-	-	0.91	0.72	0.68	0.25
$k_3$	-	-	-	0.77	0.74	0.26
$HBV$	-	-	-	-	0.97	0.39
$a_v$	-	-	-	-	-	0.36
$p$	-	-	-	-	-	-

(b)

(a) true value:  $K_1 = 0.55$ ,  $k_2 = 0.70$ ,  $k_3 = 0.25$ ,  $HBV = 0.22$ ,  $a_v = 0.72$ ,  $p = 1.00$

(b) true value:  $K_1 = 1.65$ ,  $k_2 = 0.70$ ,  $k_3 = 0.14$ ,  $HBV = 0.30$ ,  $a_v = 0.36$ ,  $p = 0.40$

of clinical datasets than the other two noise levels. Results of the global parameter identifiability study of the 6-P dual-model with image-derived arterial input for the simulated normal and HCC cases (noise level = 1) were summarized in Table IV. It could be seen that all the parameters except  $HBV$  and  $a_v$  of the simulated normal data are identifiable with one another. As mentioned above, the TAC of PV is similar with that of the surrounding liver tissue. Further, the dual blood supply of normal liver tissue is mainly from the PV ( $a_v$ : 71% ~ 92%, Table I). Therefore, it is difficult to differentiate the hepatic dual-input ( $c_b(t)$ ) from the TAC of the surrounding liver tissue using (3) in Appendix A, making  $HBV$  indistinguishable with  $a_v$ . With smaller  $a_v$  value (HCC case), the hepatic dual-input would be significantly different from the TAC of the surrounding liver tissue, and then  $HBV$  would be identifiable with  $a_v$  [Table IV (b)], which is very meaningful in clinical diagnosis of HCC. Parameter  $p$ , the only parameter to calculate the PV curve, could be identified from other parameters of the 6-P dual-model. Therefore, the 6-P dual-model could account for the hepatic dual blood supply.

#### IV. CONCLUSION

In this work, two dual-models, both consisting of the established  $^{11}\text{C}$ -acetate liver model and the hepatic DI model (accounting for the dual hepatic blood supply), were proposed. Compared with the “Golden standard”, the 6-P dual-model

could provide comparable estimates of the two HCC indicators, acceptable estimation reliability of  $a_v$  and much more reliable estimation of  $LHMRAct$  ( $K$ ), revealing that the 6-P dual-model could successfully account for the hepatic dual blood supply, which is a very challenging task for the “Golden standard”. The 6-P dual-model is more suitable than the 7-P dual-model in terms of estimation reliability and “goodness of fit” criteria. The simulation study suggests that all the parameters of the 6-P dual-model could be estimated reliably and accurately, especially for the two HCC indicators. Therefore, the 6-P dual-model structure demonstrates an appropriate transient system response and suggests a better way for the quantification of  $^{11}\text{C}$ -acetate PET studies in liver without PV curve extraction.

#### APPENDIX A $^{11}\text{C}$ -ACETATE LIVER MODEL

The differential equations for the  $^{11}\text{C}$ -acetate liver kinetic model shown in Fig. 1 are

$$\frac{dc_e(t)}{dt} = K_1 c_b(t) - (k_2 + k_3) c_e(t) \quad (\text{A1})$$

$$\frac{dc_m(t)}{dt} = k_3 c_e(t) \quad (\text{A2})$$

$$c_T(t) = c_e(t) + c_m(t) + HBV \times c_b(t) \quad (\text{A3})$$

where  $c_e(t)$  is the free  $^{11}\text{C}$ -acetate concentration in the intracellular space,  $c_m(t)$  is the intracellular  $^{11}\text{C}$ -acetate products/metabolites concentration,  $c_T(t)$  is the observed total tissue activity,  $K_1 - k_3$  are the rate constants, and  $HBV$  (hepatic blood volume) is to account for the contribution of  $^{11}\text{C}$ -acetate within vascular/sinus space of liver tissue to the observed total tissue activity. In terms of macroparameters,  $c_T(t)$  could be expressed as

$$c_T(t) = (B_1 + B_2 e^{-L_1 t}) \otimes c_b(t) + HBV \times c_b(t) \quad (\text{A4})$$

where

$$B_1 = \frac{K_1 k_3}{k_2 + k_3}$$

$$B_2 = \frac{K_1 k_2}{k_2 + k_3}, \quad L_1 = k_2 + k_3$$

are the macroparameters of the model and  $\otimes$  denotes the operation of temporal convolution.

#### APPENDIX B GNLS ESTIMATION PROCEDURE FOR THE $^{11}\text{C}$ -ACETATE DUAL-MODEL

$^{11}\text{C}$ -acetate is metabolized irreversibly in liver cells with a rate constant of  $k_3$  during the scanning period [7], therefore, beyond the dynamic phase of the hepatic arterial and portal venous blood flow, the ratio of  $c_T(t)$  (the observed total tissue activity) to  $c_b(t)$  (the model dual-input function) could be described by

$$\frac{c_T(t)}{c_b(t)} = \frac{K}{c_b(t)} \int_0^t c_b(\tau) d\tau + \frac{K_1 k_2}{(k_2 + k_3)^2} + HBV \quad (\text{B1})$$

where

$$K = \frac{K_1 k_3}{k_2 + k_3}.$$

As shown in (A4) of Appendix A,  $B_1$  has the same form as the forward clearance  $K$  ( $K = K_1 k_3 / (k_2 + k_3)$ ), therefore, it might be very useful to obtain  $B_1$  by a graph of the ratio of the total tracer concentration in tissue to the tracer concentration in blood versus the ratio of the blood tracer concentration time integral to the tracer multiple-time activity data in blood. The GNLS approach applied to the dual-model of  $^{11}\text{C}$ -acetate is a cascaded estimation algorithm, which has three steps shown in Fig. 2. In the first step, linear graphical analysis was applied to estimate  $B_1$  by (B1). The ratio of  $c_T(t)$  to  $c_b(t)$  changes rapidly during the dynamic phase of the tracer activity in blood, therefore, the data to be fitted should belong to the input steady-state space. In this study, the fitting period was from 3 min to 10 min since image-derived time-activity curves of the hepatic arteries and portal vein imply that  $^{11}\text{C}$ -acetate concentrations in the blood (HA and PV) are in steady-state with tissue free  $^{11}\text{C}$ -acetate by 3 min. To calculate the dual-input function  $c_b(t)$  in (B1) for the first iteration,  $a_v$  was empirically set to be 0.8 according to its mean value of the nontumor liver tissue in [8],  $p$  and  $E$  was set to their initial guesses. During the graphical fitting period, the two blood TACs are almost virtually identical [9], therefore, the estimated  $B_1$  is less affected by the actual PV contribution ratio ( $a_v$ ). Furthermore, it is well accepted that the estimates by the linear graphical analysis are very robust. Thereby, it is reasonable to consider the estimated  $B_1$  by step 1 as a *prior* for the subsequent estimation schemes. In the second step, the weighted NLS algorithm was utilized to estimate  $HBV$ ,  $a_v$ ,  $p$ ,  $E$  and the other two macroparameters:  $B_2$  and  $L_1$  (Appendix A) with the known  $B_1$ , which aims to minimize the weighted residual sum of squares (WRSS). The weight used in this step was

$$w_i = \frac{\Delta t_i}{c_T(t_i)} \quad i = 1, 2, \dots, 25 \quad (\text{B2})$$

where  $\Delta t_i = t'_i - t'_{i-1}$  is the scanning interval and  $c_T(t_i)$  (decay corrected) is the total tracer concentration in tissue at the mid-times of sampling time  $t'_i$ . As seen in Fig. 2, the first two steps would not cease until the difference between the estimated  $a_v$  in step 2 and the initial value of  $a_v$  utilized in step 1 is less than 0.2 and the difference between the estimated  $(p + E)$  in step 2 and its initial value utilized in step 1 is less than 0.2. In the successive iteration, the initial values of  $a_v$ ,  $p$  and  $E$  would be set to their latest estimates to calculate the dual-input function. In the third step, parameter  $K$  (same as another HCC marker: the “local hepatic metabolic rate-constant of acetate ( $LHMRAct$ )”) would be estimated by linear regression using the most updated  $a_v$ ,  $p$  and  $E$  values to calculate the dual-input function.

#### ACKNOWLEDGMENT

The authors would like to thank Dr. C.-L. Ho of the Department of Nuclear Medicine and PET, Hong Kong Sanatorium and Hospital.

## REFERENCES

- [1] S. Okazumi, K. Isono, K. Enomoto, T. Kikuchi, M. Ozaki, H. Yamamoto, H. Hayashi, T. Asano, and M. Ryu, "Evaluation of liver tumors using fluorine-18-fluorodeoxyglucose PET: Characterization of tumor and assessment of effect of treatment," *J. Nucl. Med.*, vol. 33, no. 3, pp. 333–339, 1992.
- [2] T. Torizuka, N. Tamaki, T. Inokuma, Y. Magata, Y. Yonekura, A. Tanaka, Y. Yamaoka, K. Yamamoto, and J. Konishi, "Value of fluorine-18-FDG-PET to monitor hepatocellular carcinoma after interventional therapy," *J. Nucl. Med.*, vol. 35, no. 12, pp. 1965–1969, 1994.
- [3] T. Torizuka, N. Tamaki, T. Inokuma, Y. Magata, S. Sasayama, Y. Yonekura, A. Tanaka, Y. Yamaoka, K. Yamamoto, and J. Konishi, "In vivo assessment of glucose metabolism in hepatocellular carcinoma with FDG-PET," *J. Nucl. Med.*, vol. 36, no. 10, pp. 1811–1817, 1995.
- [4] C. Ho, C. Yu, and D. Yeung, " $^{11}\text{C}$ -acetate PET imaging in hepatocellular carcinoma and other liver masses," *J. Nucl. Med.*, vol. 44, no. 2, pp. 213–221, 2003.
- [5] D. Delbeke and C. Pinson, " $^{11}\text{C}$ -acetate: A new tracer for the evaluation of hepatocellular carcinoma," *J. Nucl. Med.*, vol. 44, no. 2, pp. 222–223, 2003.
- [6] G. Brix, S. I. Ziegler, M. E. Bellemann, J. Doll, R. Schosser, R. Lucht, H. Krieter, D. Nosske, and U. Haberkorn, "Quantification of [ $^{18}\text{F}$ ]FDG uptake in the normal liver using dynamic PET: Impact and modeling of the dual hepatic blood supply," *J. Nucl. Med.*, vol. 42, no. 8, pp. 1265–1273, 2001.
- [7] S. Chen, C. Ho, D. Feng, and Z. Chi, "Tracer kinetic modeling of  $^{11}\text{C}$ -acetate applied in the liver with positron emission tomography," *IEEE Trans. Med. Imag.*, vol. 23, no. 4, pp. 426–432, Apr. 2004.
- [8] S. Chen and D. Feng, "Noninvasive quantification of the differential portal and arterial contribution to the liver blood supply from PET measurements using  $^{11}\text{C}$ -acetate kinetic model," *IEEE Trans. Biomed. Eng.*, vol. 51, no. 9, pp. 1579–1585, Sep. 2004.
- [9] O. L. Munk, L. Bass, K. Roelsgaard, D. Bender, S. B. Hansen, and S. Keiding, "Liver kinetics of glucose analogs measured in pigs by PET: Importance of dual-input blood sampling," *J. Nucl. Med.*, vol. 42, no. 5, pp. 795–801, 2001.
- [10] J. Correia, "Editorial: A bloody future for clinical PET," *J. Nucl. Med.*, vol. 33, no. 4, pp. 620–622, 1992.
- [11] L. N. Weinberg, S. C. Huang, E. J. Hoffman, L. Araujo, C. Nienaber, M. GroverMcKay, M. Dahlbom, and H. Schelbert, "Validation of PET-acquired input functions for cardiac studies," *J. Nucl. Med.*, vol. 29, no. 2, pp. 241–247, 1988.
- [12] T. Ohtake, N. Kosaka, T. Watanabe, I. Yokoyama, T. Moritan, M. Masuo, M. Iizuka, K. Kozeni, T. Momose, S. Oku, J. Nishikawa, Y. Sasaki, and M. Iio, "Noninvasive method to obtain input function for measuring tissue glucose utilization of thoracic and abdominal organs," *J. Nucl. Med.*, vol. 32, no. 7, pp. 1432–1438, 1991.
- [13] G. Germano, B. C. Chen, S.-C. Huang, S. S. Gambhir, E. J. Hoffman, and M. E. Phelps, "Use of the abdominal aorta for arterial input function determination in hepatic and renal PET studies," *J. Nucl. Med.*, vol. 33, no. 4, pp. 613–620, 1992.
- [14] K. Chen, D. Bandy, E. Reiman, S.-C. Huang, M. Lawson, D. Feng, L. Yun, and A. Palant, "Noninvasive quantification of the cerebral metabolic rate for glucose using positron emission tomography,  $^{18}\text{F}$ -fluoro-2-deoxyglucose, the patlak method, and an image-derived input function," *J. Cereb. Blood Flow Metab.*, vol. 18, pp. 716–723, 1998.
- [15] X. Li, D. Feng, K. Lin, and S. C. Huang, "Estimation of myocardial glucose utilisation with PET using the left ventricular time-activity curve as a noninvasive input function," *Med. Bio. Eng. Comput.*, vol. 36, no. 1, pp. 112–117, 1998.
- [16] L. M. Wahl, M.-C. Asselin, and C. Nahmias, "Regions of interest in the venous sinuses as input functions for quantitative PET," *J. Nucl. Med.*, vol. 40, no. 10, pp. 1666–1675, 1999.
- [17] H.-M. Wu, C. K. Hoh, Y. Choi, H. R. Schelbert, R. A. Hawkins, M. E. Phelps, and S.-C. Huang, "Factor analysis for extraction of blood time-activity curves in dynamic FDG-PET studies," *J. Nucl. Med.*, vol. 36, no. 9, pp. 1714–1721, 1995.
- [18] M. Naganawa, Y. Kimura, and A. Matani, "Modification of ICA for extracting blood vessel-related component in nuclear medicine: Contrast function and nonnegative constraints," in *Proc. 4th Int. Symp. Independent Component Analysis and Blind Signal Separation*, pp. 65–70.
- [19] D. Feng, S. C. Huang, and X. Wang, "Models for computer simulation studies of input functions for tracer kinetic modeling with positron emission tomography," *Int. J. Biomed. Comput.*, vol. 32, pp. 95–110, 1993.
- [20] A. M. Peters and M. J. Myers, *Physiological Measurements with Radionuclides in Clinical Practice*. Oxford, U.K.: Oxford Univ. Press, 1998.
- [21] J. O. Rowan, *Physics and the Circulation*. Bristol, U.K.: Adam Hilger, 1981.
- [22] S. Chen and D. Feng, "Novel parameter estimation methods for  $^{11}\text{C}$ -acetate dual-input liver model with dynamic PET," *IEEE Trans. Biomed. Eng.*, vol. 53, no. 5, pp. 967–973, May 2006.
- [23] C. S. Patlak, R. G. Blasberg, and J. D. Fenstermacher, "Graphical evaluation of blood-to-brain transfer constants from multiple-time uptake data," *J. Cereb. Blood Flow Metab.*, vol. 3, pp. 1–7, 1983.
- [24] P. Vanrolleghem and D. Dochain, "Bioprocess model identification," in *Advanced Instrumentation, Data Interpretation, and Control of Biotechnological Process*, J. Van Impe, P. Vanrolleghem, and D. Iserentant, Eds. Norwell, MA: Kluwer, 1998, pp. 251–318.
- [25] M. Rodriguez-Fernandez, J. A. Egea, and J. R. Banga, "Novel meta-heuristic for parameter estimation in nonlinear dynamic biological systems," *BMC Bioinf.*, vol. 7, pp. 483–500, 2006.
- [26] H. Akaike, "A new look at the statistical model identification," *IEEE Trans. Autom. Control*, vol. AC-19, no. 6, pp. 716–723, Dec. 1974.
- [27] G. Schwarz, "Estimating the dimension of a model," *Ann. Statist.*, vol. 6, pp. 461–564, 1978.